## PAPER

Check for updates

# Unusual enhancement in efficiency of DSSCs upon modifying photoanodes with reduced graphene oxide†

Sujit Bhand, Plawan Kumar Jha and Nirmalya Ballav [iD] *

Reduced graphene oxide (rGO) has emerged as an excellent interfacial material for improvising the performance of dye-sensitized solar cells (DSSC). Herein, we have applied rGO as interfacial layers between a fluorine doped tin oxide (FTO) coated glass substrate and semiconducting material $TiO_2$ in a photoanode of a DSSC which showed an unusual enhancement in generating a photocurrent in comparison to the control (without rGO layers). An electrochemical impedance spectroscopy (EIS) study was performed to gain the mechanistic insights into such a remarkable enhancement of photoelectric conversion efficiency (PCE) which revealed improved charge transfer and suppressed charge recombination due to high-electrical conductivity and probably more negative work function of our rGO material compared to the bare $TiO_2$ photoanode.

## Introduction

In view of the extensive demand for non-renewable energy, dye-sensitized solar cells (DSSCs) continue to be promising, perhaps due to their easy fabrication and affordability.[1,2] A typical DSSC comprises three main components: (a) working electrode-photoanode (usually $TiO_2$ nanocrystalline film), (b) counter electrode (conducting glass), and (c) electrolyte (iodine/triiodide $(I^-/I_3^-)$ redox couple).[3,4] Recently, various semiconducting nanomaterials have been explored as photoanodes[5,6] and counter electrodes[7–9] to improve the overall performance of DSSCs. The interfaces in a DSSC device, particularly on the photoanode side play crucial roles in the charge separation and transport. Specifically, electrons generated from the excited dye molecules are separated at the $TiO_2$/dye interface, and subsequently passed through the mesoporous crystalline semiconductor material to the current collector.

The interface associated with transparent conducting glass such as fluorine-doped tin oxide (FTO) and $TiO_2$ is extremely important as it creates a conducting path for the electrons in the device. Also, at this location, the possibility of electron–hole recombination is very high which ultimately hampers the performance of the DSSC. Fig. 1 presents the schematic representation of a DSSC device depicting various interfaces and charge movement. Applying various nanomaterials, such as, graphene,[10–14] carbon nanotubes (CNT)[13,14] and gold/platinum nanoparticles[15] in a photoanode could reduce the rate of

charge recombination, therefore, improved the PCE of DSSCs.[16] Out of which, graphene-based materials possessing excellent physicochemical properties have emerged as promising candidates for the enhancement of the efficiency of DSSC. In the combination of $TiO_2$ and functionalized graphene materials, such as, reduced graphene oxide (rGO), the electron transfer rate increases at the interface.[17] However, blending micron size rGO nanosheets along with nanosized (<25 nm) porous $TiO_2$ could introduce more grain boundaries in the layer which in turn could obstruct the charge flow and underestimate the efficiency of DSSC.[18] In the context of such interface engineering in DSSC with rGO an inevitable question is: how important is the quality of rGO? Also, there are numerous investigations on DSSC,[19,20] whereby the FTO surface was decorated with a compact thin layer of $TiO_2$ made from $TiCl_4$; however, such films are air and moisture sensitive and can degrade over time, therefore ambient stability is an unavoidable issue.

Herein, we have modified the FTO/$TiO_2$ interface by self-healed rGO generated from rather unconventional wet-chemical reduction methods. Specifically, rGOs with distinctive two-dimensional (2D) and three-dimensional (3D) morphological patterns, rGO1 (GO to rGO reduction was done with the Fe(II) salt)[21] and rGO2 (GO to rGO reduction was done with the Cu(I) salt),[22] respectively, were explored. A schematic view of our DSSC involving interfacial rGO layers along with FESEM images of rGO1 and rGO2 is presented in Fig. 1. The interfacial layers of rGO on the FTO can behave as an extended electron collecting electrode, as successfully demonstrated by Chen *et al.*,[17] eventually improving the electron-transport rate in DSSC. As a result, the PCE values of our DSSC devices fabricated at ambient conditions were realized to be noticeably higher than previous reports which is the primary highlight of the

*Department of Chemistry, Indian Institute of Science Education and Research (IISER), Dr Homi Bhabha Road, Pune, 411 008, India. E-mail: nballav@iiserpune.ac.in*

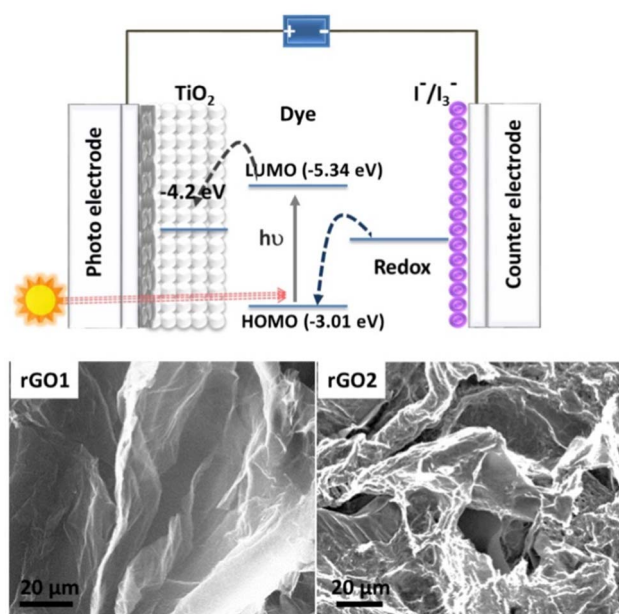† Electronic supplementary information (ESI) available. See DOI: https://doi.org/10.1039/d2ra05375f

Fig. 1 Schematic representation of a DSSC device depicting interfaces and charge movements (above). It is clear from the alignment of various energy levels, rGO introduced in between FTO and $TiO_2$ could facilitate electron transfer from $TiO_2$ layer to FTO current collector. Field-emission scanning electron microscopy (FESEM) images of rGO1 and rGO2 showing different morphological patterns (below).

present study. An easy comparison of the present work over earlier literature can be assessed from Table S1.†

## Results and discussion

A transparent FTO coated glass was cleaned in soap solution using an ultrasonic bath for 15 min, followed by rinsing and sonication in deionized water. After such three consecutive cleaning, the FTO coated glass was finally rinsed with isopropanol (IPA), heated in a furnace for 15 min at 200 °C, and finally used for the fabrication of DSSC prototype devices D1, D2, D3 and D4.

D1: bare FTO coated glass was used as the current collector. D2: FTO coated glass was kept in the 50 mM aqueous solution of $TiCl_4$ at 70 °C for 15 min followed by 30 min heating at 125 °C. D3: ~1 mg/1.5 mL dispersion of rGO1 (30 min sonication in $N$-methylpyrrolidone (NMP) was coated on FTO coated glass by spin coating method (800 rpm s$^{-1}$; 60 s) and dried by heating at 200 °C for 10 min. D4: similar as D3 just rGO2 was used instead of rGO1. About 7–10 μm thick transparent $TiO_2$ was doctor-bladed over treated FTO substrate, kept steady at room temperature for 10 min, and heated at 125 °C for 15 s. After that 16 μm thick layer of opaque $TiO_2$ paste was coated using the doctor-blade method, kept for 5 min at room temperature, then sintered at 350 °C for 15 min, 450 °C for 30 min and 500 °C for 30 min. For the dye absorption, photoelectrodes were immersed in 0.3 mM N719 dye (in ethanol) for 3 h at room temperature followed by thorough rinsing with ethanol to remove excess dye and dried in air. For the device assembly, photoanode and

conductive platinised-glass counter electrode (with hole diameter of 0.75 mm) were sandwiched and sealed with 60 μm thermoplastic Surlyn spacer at 100 °C for 10 s. The commercial iodine-based liquid electrolyte was introduced into the sandwich cells through holes in the counter electrode. Please note that, the PCE values shown in Table 1 is the average of 10 devices and the % PCE of all fabricated devices are presented in Fig. S5.† To estimate loading of dye, photoanode was kept in 10 mL ethanol and aqueous NaOH (1 M) solution and absorption spectra recorded.[12]

The FESEM images showed micron-sized and well-distributed rGO1 and rGO2 on the rGO treated FTO, without any significant change in surface morphologies, though, heated at high-temperature (Fig. S1†). Characteristic signatures of the D and G band in the Raman spectra is evidenced of the fact that rGO backbones were primarily retained even after the heat treatment (Fig. S2a†). The coating of $TiO_2$ (both transparent and opaque mesoporous layers) was observed to be around 23 μm thick without any cracking and peeling even after annealing at ~500 °C (Fig. S3 and S4†). The light transmission properties of the FTO in all the devices were evaluated by the solid-state UV-vis spectroscopy (Fig. S2b†). About 84% transmittance was observed for bare the FTO (D1). Interestingly, the transparency was almost maintained after successful integration of the interfacial layers of rGOs (~82–83%) which suggests that the photosensitizer dye in DSSC devices could be well-illuminated without severe photon loss during the measurements. Solid-state absorption spectra of dye decorated photoanode revealed characteristic electronic transition signatures of N719 (Fig. S6†).

Performance of the DSSC devices D1, D2, D3 and D4 were realised under 1 sun illumination. The short circuit current density ($J_{SC}$), open circuit voltage ($V_{oc}$), fill factor (FF), and power conversion efficiency (PCE) for D1 was found to be around 14.88 mA cm$^{-2}$, 0.7 V, 0.57, and 6.08% respectively (Table 1 and Fig. 2b). Interestingly, after the rGO modification (D3) the $J_{SC}$ increased dramatically to 17.89 mA cm$^{-2}$, resulting in the PCE value of 8.08%.

Such an enhancement clearly evidenced an alteration of the interfacial energy alignment upon incorporation of the rGO even with distinctive morphological patterns. As our synthesized rGO (rGO1) is defect-healed so a higher number of generated electrons at the upper layer (dye) could be easily facilitated towards FTO. Also, due to the distinct work function value of rGO and $TiO_2$ the electron is unable to travel back towards $TiO_2$ leading to higher electron generation as realized from the values of $J_{SC}$. Although reported rGOs were made by

Table 1 Photovoltaic performance summary of the DSSC devices

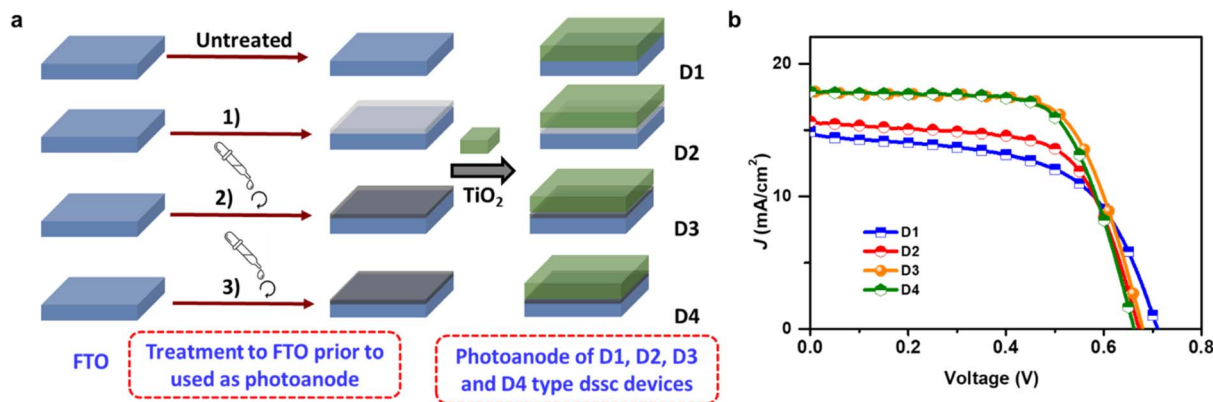|  | D1 | D2 | D3 | D4 |
| --- | --- | --- | --- | --- |
|  | Blank | $TiCl_4$ | rGO1 | rGO2 |
| $J_{SC}$ (mA cm$^{-2}$) | 14.88 | 15.65 | 17.89 | 17.91 |
| $V_{oc}$ (V) | 0.70 | 0.67 | 0.66 | 0.66 |
| Fill factor (FF) | 0.57 | 0.64 | 0.67 | 0.67 |
| % efficiency | 6.08 ± 0.5 | 6.80 ± 0.5 | 8.08 ± 0.2 | 8.01 ± 0.3 |

Fig. 2 (a) Schematic representation of preparation of photoanode for device type D1, D2, D3 and D4; (1) $TiCl_4$ treatment followed by calcination to fabricate thin $TiO_2$ blocking layer (2) spin coating of rGO1 (3) spin coating of rGO2. (b) Current density–voltage ($J$–$V$) curves for the DSSCs obtained from different compositions at the FTO/$TiO_2$ interface. Device active area was ~0.64 cm$^2$ and all measurements were performed under light source 100 mW cm$^{-1}$ (1 sun).

conventional reducing agents, the PCE value of the graphene modified DSSCs is comparable or lower than here reported results (Table S1†) which validates the importance of use of reduced graphene oxide and method of applying rGO on surface instead of using it in $TiO_2$ paste. On the other hand, the PCE of D2 and D4 found to be 6.80 and 8.01% respectively emphasizing the significance of rGO at the interfaces of $TiO_2$/FTO.

Considering the fact that the minute changes in interfacial resistance greatly alter the DSSCs performance, electrochemical impedance spectroscopy (EIS) measurements were performed. Upon fitting the Nyquist plots by the equivalent circuit (as shown in Fig. 3), two semicircles appeared that can be assigned as resistance 1 ($R_1$, first) and resistance 2 ($R_2$, second). The intercept at real $Z$-axis is the equivalent series resistance ($R_s$) showing the total resistance created by the internal components of DSSC. $R_s$ of the D3 and D4 was found to be ~30.4 and 34.0 Ω, respectively, which is slightly higher than control devices (D1 and D2) (Table 2). Also, the $R_s$ of D3 was found to be lower than D4 which could be due to the higher electrical conductivity of rGO1 (500 S m$^{-1}$)[21] compared to rGO2 (150 S m$^{-1}$)[22] ultimately affecting the $J_{SC}$ and PCE.

The interface between electrolyte and counter electrode was unaltered for all the devices therefore $R_1$ (2.1, 1.2, 1.7, 2.1 Ω for D1, D2, D3, D4, respectively) was realised to be similar except for

Table 2 Extracted parameters from the Nyquist plots

| Device | $R_s$ [Ω] | $R_2$ [Ω] | $\omega_{max}$ [Hz] | $\tau_e$ |
|---|---|---|---|---|
| D1 | 22.8 | 10.2 | 52 | 3.06 |
| D2 | 29.1 | 7.5 | 48 | 3.31 |
| D3 | 30.4 | 10.4 | 45 | 3.54 |
| D4 | 34.0 | 9.1 | 46 | 3.46 |

D2 where $TiO_2$ layer prepared by chemical method acted as a blocking layer. $R_2$ is the resistance created at the electrolyte/dye/$TiO_2$ interface which is found to be 10.2, 7.5, 10.4, and 9.1 Ω for devices D1, D2, D3, and D4, respectively. The lowest $R_2$ value of D2 is because $TiO_2$ prepared from specific concentration[23] of $TiCl_4$.

The electron lifetime ($\tau_e$) can be expressed as $\tau_e = 1/(2\pi\omega_{max})$ where $\omega_{max}$ is the maximum frequency calculated from the semicircle. For D1 and D2 the $\tau_e$ values were found to be around 3.06 and 3.31 ms, respectively, however, after the rGO coating, the $\tau_e$ of device D3 and D4 increased to 3.54 and 3.46 ms, respectively, which clearly endorsing the importance of rGO on the reduction of charge-recombination process[24] in DSSC. Furthermore, the absorption spectra of dye de-absorption solution from photoanode revealed that the dye loading was almost similar across the devices (Fig. S7†). Overall, it can be concluded that mere spin coating of rGO at the $TiO_2$/FTO interface is good enough for enhancing the performance of DSSC devices.

## Conclusions

In summary, we have chemically modified the FTO/$TiO_2$ interface of DSSC by self-healing rGO materials. Optical transparency of the photoanode was almost retained in such an interfacial modification. As assembled DSSC showed the PCE values ~8% which is more than ~2% compared to the device without the interfacial rGO layers. The EIS measurement on our interface engineered DSSCs revealed that the enhancement of
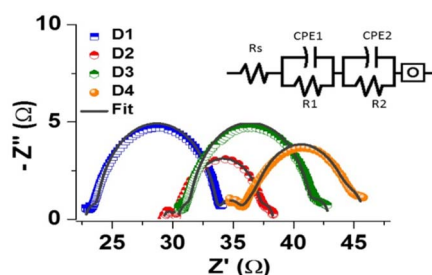


Fig. 3 Typical Nyquist plots obtained from the DSSC devices D1, D2, D3 and D4. Experimental data points were fitted with an equivalent circuit schematically shown in the inset.

PCE is mainly due to enhanced electron transfer and suppressed charge recombination process at the FTO/TiO$_2$ interface.

## Conflicts of interest

There are no conflicts to declare.

## Acknowledgements

## Notes and references

1 M. Grätzel, *Acc. Chem. Res.*, 2009, **42**, 1788–1798.

2 B. O'Regan and M. Grätzel, *Nature*, 1991, **353**, 737–740.

3 T. Le Bahers, T. Pauporté, P. P. Lainé, F. Labat, C. Adamo and I. Ciofini, *J. Phys. Chem. Lett.*, 2013, **4**, 1044–1050.

4 H. Tian, J. Gardner, T. Edvinsson, P. B. Pati, J. Cong, B. Xu, M. Abrahamsson, U. B. Cappel and E. M. Barea, in *Solar Energy Capture Materials*, The Royal Society of Chemistry, 2019, pp. 89–152.

5 J. Bisquert, D. Cahen, G. Hodes, S. Rühle and A. Zaban, *J. Phys. Chem. B*, 2004, **108**, 8106–8118.

6 K. Fan, J. Yu and W. Ho, *Mater. Horiz.*, 2017, **4**, 319–344.

7 P. Hasin, M. A. Alpuche-Aviles, Y. Li and Y. Wu, *J. Phys. Chem. C*, 2009, **113**, 7456–7460.

8 J. Wu, Z. Lan, J. Lin, M. Huang, Y. Huang, L. Fan, G. Luo, Y. Lin, Y. Xie and Y. Wei, *Chem. Soc. Rev.*, 2017, **46**, 5975–6023.

9 S. Vijaya, G. Landi, J. J. Wu and S. Anandan, *J. Power Sources*, 2020, **478**, 229068.

10 Y. Kusumawati, M. A. Martoprawiro and T. Pauporté, *J. Phys. Chem. C*, 2014, **118**, 9974–9981.

11 P. E. Marchezi, G. G. Sonai, M. K. Hirata, M. A. Schiavon and A. F. Nogueira, *J. Phys. Chem. C*, 2016, **120**, 23368–23376.

12 D. Cao, A. Wang, X. Yu, H. Yin, J. Zhang, B. Mi and Z. Gao, *J. Colloid Interface Sci.*, 2021, **586**, 326–334.

13 S. Aseena, N. Abraham and V. S. Babu, *Ceram. Int.*, 2020, **46**, 28355–28362.

14 S. Zhang, H. Niu, Y. Lan, C. Cheng, J. Xu and X. Wang, *J. Phys. Chem. C*, 2011, **115**, 22025–22034.

15 P. Dong, C. L. Pint, M. Hainey, F. Mirri, Y. Zhan, J. Zhang, M. Pasquali, R. H. Hauge, R. Verduzco, M. Jiang, H. Lin and J. Lou, *ACS Appl. Mater. Interfaces*, 2011, **3**, 3157–3161.

16 M. Janani, P. Srikrishnarka, S. V. Nair and A. S. Nair, *J. Mater. Chem. A*, 2015, **3**, 17914–17938.

17 T. Chen, W. Hu, J. Song, G. H. Guai and C. M. Li, *Adv. Funct. Mater.*, 2012, **22**, 5245–5250.

18 L. Wei, S. Chen, Y. Yang, Y. Dong, W. Song and R. Fan, *RSC Adv.*, 2016, **6**, 100866–100875.

19 F. Kabir, S. Nazmus Sakib, S. Shehab Uddin, E. Tawsif Efaz and M. T. Farhan Himel, *Sustain. Energy Technol. Assess.*, 2019, **35**, 298–307.

20 Z. Han, Z. Zhao, Z. Du, L. Zhao and X. Cong, *Mater. Lett.*, 2014, **136**, 424–426.

21 P. K. Jha, S. K. Singh, V. Kumar, S. Rana, S. Kurungot and N. Ballav, *Chem*, 2017, **3**, 846–860.

22 P. K. Jha, K. Gupta, A. K. Debnath, S. Rana, R. Sharma and N. Ballav, *Carbon*, 2019, **148**, 354–360.

23 H. K. Adli, T. Harada, S. Nakanishi and S. Ikeda, *Phys. Chem. Chem. Phys.*, 2017, **19**, 26898–26905.

24 N. Yang, J. Zhai, D. Wang, Y. Chen and L. Jiang, *ACS Nano*, 2010, **4**, 887–894.